Current Biology, Vol. 12, 1891–1899, November 19, 2002, ©2002 Elsevier Science Ltd. All rights reserved. PII S0960-9822(02)01276-9

Converging Populations of F-Actin Promote Breakage of Associated Microtubules to Spatially Regulate Microtubule Turnover in Migrating Cells

Stephanie L. Gupton, Wendy C. Salmon, and Clare M. Waterman-Storer[1]
Department of Cell Biology and
Institute for Childhood and Neglected Diseases
The Scripps Research Institute
La Jolla, California 92037

Summary

Background: In migrating cells, the retrograde flow of filamentous actin (f-actin) from the leading edge toward the cell body is accompanied by the synchronous motion of microtubules (MTs, [1]), whose plus ends undergo net growth. Thus, MTs must depolymerize elsewhere in the cell to maintain polymer mass over time. The source and location of depolymerized MTs is unknown. Here, we test the hypothesis that MT polymer loss occurs in central cell regions and is induced by the convergence of actin retrograde and anterograde flow, which buckles and breaks associated MTs and promotes minus-end depolymerization.
Results: We characterized the effects of calyculin A and ML-7 on the movement of f-actin and MTs by multispectral fluorescence recovery after photobleaching (FRAP) and fluorescent speckle microscopy (FSM). Our studies show that these drugs affect the rate of f-actin and MT convergence and MT buckling in a central cell region we call the "convergence zone." Increases in f-actin convergence are associated with faster MT turnover and an increase in both MT breakage and minus-end depolymerization, but they have no effect on MT plus end dynamic instability.
Conclusions: We propose that f-actin movement into the convergence zone plays a major role in spatially modulating MT turnover during cell migration by regulating MT breakage, and thus minus-end dynamics, in central cell regions.

Introduction

Directed locomotion of tissue cells requires complex interactions between actin filaments (f-actin) and microtubules (MTs) (reviewed in [2]). Actin organization, assembly dynamics, and movement are highly polarized in migrating tissue cells (Figure 1A; [1, 3]). Actin polymerizes into a dense filament network at the leading cell edge and moves retrograde through the lamellipodium [1, 3, 4]. Actin flow rate slows at the junction between the lamellipodium and lamellum and continues through the lamellum at the reduced rate [5, 1]. In the cell body, f-actin at the dorsal cell surface often forms bundles that move in an anterograde direction and are probably important to forward motion of the trailing cell body [1, 6]. The opposing retrograde f-actin flow in the lamellum and anterograde f-actin movement in the cell body meet in a "convergence zone," where little directed f-actin movement occurs but where there is extensive filament disassembly [1].

The MT array in migrating cells is also polarized, with the perinulear centrosome that nucleates MTs positioned toward the leading edge and many MT plus ends emanating through the lamellum toward the leading edge [7, 2]. Lamellum MT plus ends exhibit dynamic instability, i.e., random switching between persistent phases of growth and shortening [8, 9], while undergoing concurrent acto-myosin-dependent retrograde flow [8, 10–14], which is precisely coupled to movement of the lamellum f-actin network [1, 14]. As MTs move rearward from the lamellum into the convergence zone, they often exhibit extensive buckling, bending, and breaking [1, 8, 14]. Breaking MTs produce labile, non-centrosomal MT minus ends, which usually undergo rapid depolymerization [1, 8, 14, 15]. MT movements are also coupled to f-actin bundles that move in an anterograde direction in the cell body [1].

Thus, MT assembly dynamics are regionally organized in a migrating cell [16, 17]. Because MT plus ends in the leading lamella maintain a constant distance on average from the leading edge while their shafts move rearward toward the cell center, their plus ends must undergo net growth near the leading edge [8]. Concurrently, there must be net depolymerization of MTs to maintain constant polymer mass over time. However, the source and location of the disassembling polymer is unknown. Because centrosome bound MT minus ends do not exhibit continuous disassembly [8], "treadmilling" of centrosomal MTs cannot account for this net depolymerization.

Our hypothesis is that the convergence of f-actin retrograde and anterograde flow that drives the motion of associated MTs in migrating cells induces MT buckling and breakage in the convergence zone between the lamellum and cell body and that depolymerization of the broken MT minus ends could supply tubulin dimers to feed net MT growth at the leading edge. To test the idea that f-actin convergence spatially modulates MT turnover, we used dual-wavelength fluorescence recovery after photobleaching (FRAP) [4, 18] and fluorescent speckle microscopy (FSM) [1, 19–21] to simultaneously monitor MT and actin dynamics during pharmacological manipulation of f-actin convergence. Our studies show that f-actin convergence plays a major role in spatially modulating MT turnover by regulating MT breakage, and thus minus-end dynamics, during cell migration.

Results

MT Buckling and Breakage Are Associated with Converging Populations of F-Actin

Previous studies have shown that MT bending, buckling, and breakage are common occurrences in the lamellum and convergence zone of newt lung epithelial cells but have not investigated their origin [1, 8]. To determine

[1] Correspondence: waterman@scripps.edu

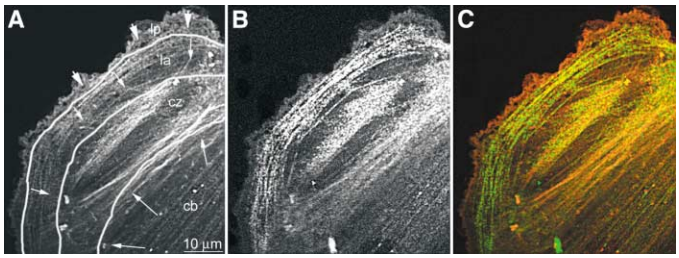

Figure 1. Newt Lung Epithelial Cell Injected with X-Rhodamine Actin and Expressed Myosin Light Chain-GFP

(A) X-rhodamine actin and cartoon representation overlay of the four functionally defined zones of f-actin movement as summarized from [1]. lp = lamellipodium, la = lamellum, cz = convergence zone, and cb = cell body. Arrows signify the direction of f-actin movement, and arrow head size denotes the relative magnitude of velocity. There is no net actin movement within the convergence zone.

(B) MLC-GFP organization.

(C) Colocalization of actin (red) and myosin (green). The scale bar represents 10 μm.

if local convergence of actin filament meshworks was associated with MT buckling, we analyzed local MT buckling events and their relation to actin dynamics in the convergence zone and in the proximal lamellum, where these events occur most often, by using dual-wavelength spinning-disk confocal FSM of newt lung cells comicroinjected with Cy2 tubulin and X-rhodamine actin [1]. Figures 2A–2D and Movie 1 demonstrate an example of MT buckling and breakage in the convergence zone. Dual-wavelength kymograph analysis (Figure 2B) showed rearward movement from the lamellum and forward movement from the cell body of both MTs and f-actin. Examination of single MTs revealed that as a proximal portion of the MT moves forward with f-actin in the cell body and its distal portion moves rearward in the lamellum, the portion of the MT spanning the convergence zone becomes compressed, buckles, and breaks (Figures 2C and 2D; Movie 1). Careful inspection of Movie 1 (or Video 3 in [1]) reveals many MT buckling events and several breakage events, as well as the appearance of free minus ends when the breakage event is not visible.

MT buckling was also associated with local singularities in f-actin speckle motion within the proximal lamellum, although MT buckling was less frequent here as compared to the convergence zone. In Figures 2E–2G, tracking of individual f-actin speckles immediately adjacent to a buckling MT showed that as f-actin speckles within the lamellum meshwork moved closer together while also undergoing retrograde flow, the length of the MT spanning the converging speckles buckled to a tight radius of curvature. The MT then broke and exposed a minus end that depolymerized. Unlike observations in fibroblasts [15], our observations never included breakage of straight or gently curved MTs. Together with our previous studies [1], these results show that local f-actin convergence is associated with MT buckling and breakage.

Because f-actin convergence is likely to be powered by a contractile myosin motor, we examined the localization and dynamics of myosin II in newt lung cells with a non-isoform-specific murine myosin II light chain coupled to green fluorescent protein (MLC-GFP). In cells that had been injected with X-rhodamine actin, MLC-GFP punctae in the lamellum moved rearward [22], and MLC-GFP was also concentrated along f-actin bundles in the convergence zone and cell body (Figure 1).

Calyculin A and ML-7 Affect F-Actin Movement into the Convergence Zone

Because MT buckling and breakage occurred frequently in the convergence zone, we wished to manipulate f-actin movement, and thus MT movement, into this region to determine if convergence affected MT breakage. Calyculin A (CA) is a type I phosphatase inhibitor known to inhibit myosin light chain phosphatase and thus promote contractility [23, 24]. ML-7 is a myosin light chain kinase inhibitor that promotes relaxation [25]. To characterize the effects of these agents, we monitored f-actin and MT dynamics by dual-wavelength confocal FSM before and after perfusion of CA (20 nM; Figure 3) or ML-7 (10 μM; Figure 4).

Kymograph analysis of dual-wavelength FSM image series showed that within 2 min after perfusion of CA, there was an increase in the rate of f-actin (from 0.338 ± 0.112 μm/min to 0.635 ± 0.389 μm/min, p= .07, n = 5 cells, 280 measurements) and MT retrograde flow (from 0.3025 ± 0.134 μm/min to 0.635 ± 0.389 μm/min, p = 5.93×10^{-16}, n= 5 cells, 267 measurements) in the lamella compared to the control (Figures 3C–3E). Lamella MTs were rapidly swept rearward into the convergence zone, where they were extensively buckled and compacted (Movie 3; Figure 3B). Otherwise, CA induced small or no detectable changes in the direction or rate of f-actin or MT movement in the lamellipodium (actin: from 1.23 ± 0.7 μm/min to 1.36 ± 0 0.76 μm/min, p = 0.25, n = 5 cells, 275 measurements; MTs: infrequently seen in the lamellipodium) or cell body (actin: from −0.20 ± 0.10 μm/min to −0.26 ± 0.11, p = 0.012, n = 5 cells, 114 measurements; MT: from −0.19 ± 0.10 μm/min to −0.15 ± 0.10 μm/min, p = 0.19, n = 2 cells, 18 measurements) (Figure 3E).

Similar analysis of cells perfused with ML-7 revealed a halt or reversal of the normally anterograde f-actin (from −0.286 ± 0.22 μm/min to −0.023 ± 0.885 μm/min, p = 0.0001, n = 6 cells, 400 measurements) and MT flow (from −0.26 ± 0.22 μm/min to 0.06 ± 0.34 μm/min, p = 0.0002, n = 3 cells, 29 measurements) in the cell body toward the convergence zone, concurrent with a dissipation of f-actin bundles and a subtle decrease in MT density in the convergence zone and cell body (Figure 4). ML-7 induced a small or nonexistant change in the rate or direction of actin or MT movement in the lamellipodium (actin: from 1.47 ± 1.46 μm/min to 1.48 ±

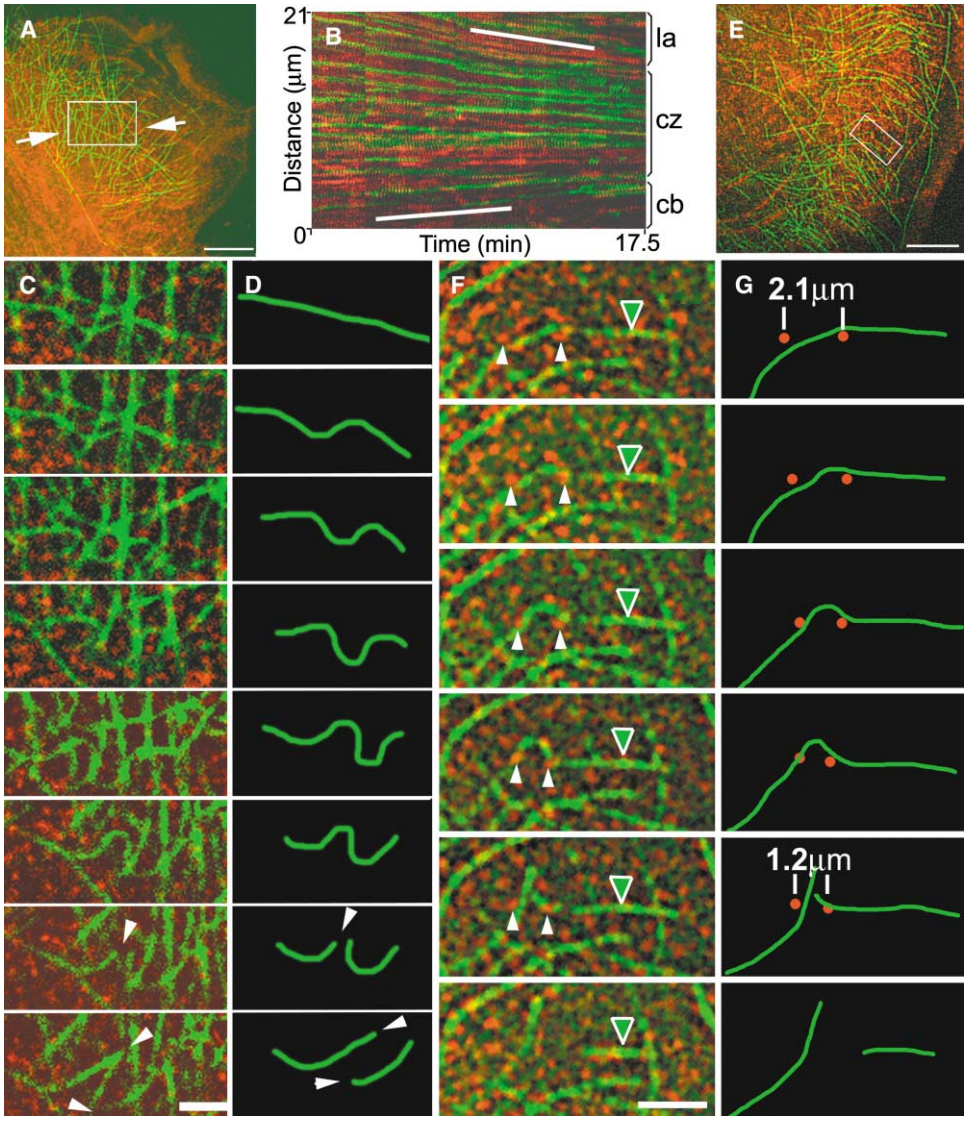

Figure 2. MT Buckling and Breakage Are Associated with Local F-Actin Convergence

Newt lung epithelial cells injected with x-rhodamine actin (red) and Cy2 tubulin (green).

(A–D) The convergence zone. (A) FSM image from a time-lapse dual-wavelength series. The box shows the region of the convergence zone from which the kymograph (B) and time series (C) were taken. Arrows indicate the direction of f-actin movement. The scale bar represents 10 μm. (B) Dual-wavelength kymograph demonstrates the converging actin and MT populations within the region of interest from (A). White lines highlight the rate and direction of cytoskeletal movement over time. la = lamellum, cz = convergence zone, and cb = cell body. (C) Time-lapse dual-wavelength confocal FSM image series from Movie 1, showing a MT in the convergence zone, bend, buckle, and break as the f-actin populations converge. Images were acquired at 10 s intervals. Arrows indicate MT breakage in the penultimate panel and the new plus and minus ends created from MT breakage in the final panel. Panel (D) is a schematic diagram highlighting the bending and breaking MT in (C).

(E–G) The proximal lamellum (E) FSM image. The boxed region shows the region extracted for time-lapse analysis in (F). (F) Dual-wavelength confocal FSM image series from Movie 2, showing a MT, become compressed, buckle, and break as the distance between two immediately adjacent f-actin speckles (arrows) is decreased by 0.8 μm over the 80 s time period (images at 10 s intervals). A bright speckle mark on the lattice (green arrowhead) of the distal MT segment stays stationary over time, indicating that the MT is shortening at the newly formed minus end. (G) Schematic diagram of the f-actin speckles (red dots) and the MT in (F). The scale bar in (C) and (F) represents 3 μm.

1.17 μm/min, $p = 0.36$, $n = 6$ cells, 450 measurements) or the lamellum (actin: from 0.335 ± 020 μm/min to 0.375 ± 0.261, $p = 0.011$, $n = 6$ cells, 390 measurements; MT: from 0.388 ± 0.247 μm/min to 0.405 ± 0.210 μm/min, $p = 0.55$, $n = 6$ cells, 62 measurements). In either CA or ML-7, MT movements occurred at the exact same rate as that of immediately adjacent f-actin speckles (our unpublished data). These results indicate that CA and ML-7 are useful reagents for simultaneously affecting f-actin and MT movement into the convergence zone and do not perturb the coupling of MT and f-actin movements.

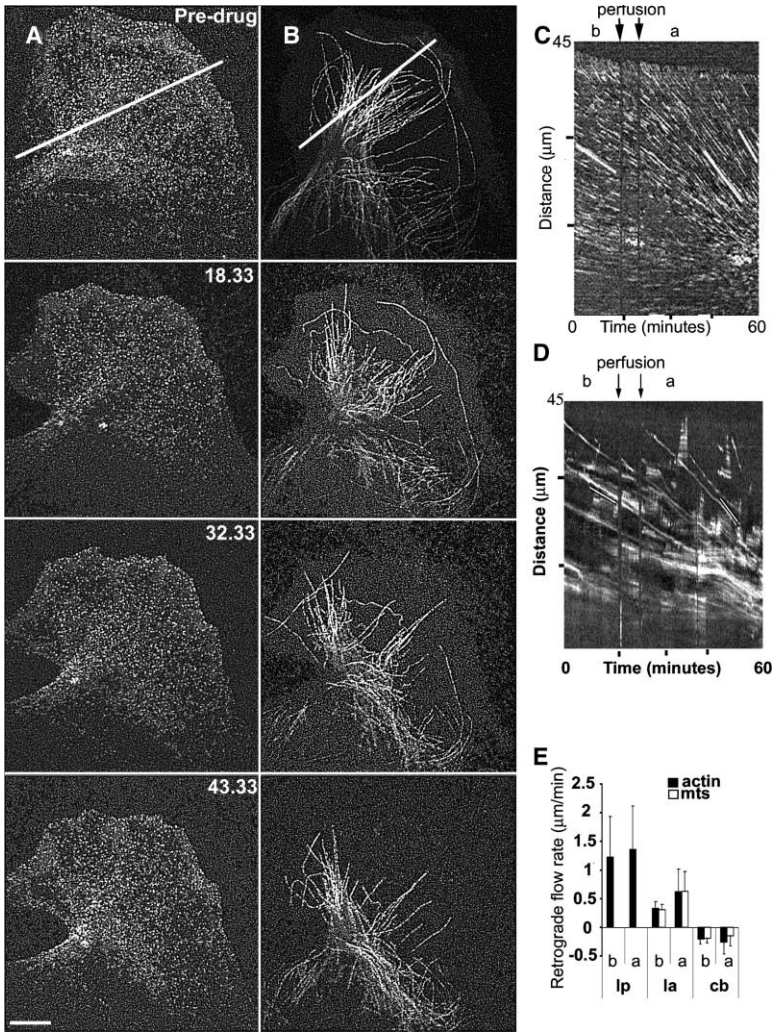

Figure 3. CA Increases the Rate of F-Actin and MT Retrograde Flow in the Lamellum

Dual wavelength FSM time-lapse image series of X-rhodamine f-actin ([A], left column) and Cy2 MTs ([B], right column) before and after perfusion with 20 nM CA. Time in minutes after perfusion is noted in the right corner of the images in (A). See Movie 3. CA causes MTs to be swept away from the leading edge and compacted in the convergence zone. White lines in (A) and (B) mark the line along which kymographs were created in (C) and (D). (C, D) Kymograph analysis of X-rhodamine f-actin speckles (C) and Cy2 MTs (D) shows that the rate of retrograde flow into the lamellum increases after perfusion with CA. Lines highlight the rates of speckle motion. lp = lamellipodium, la = lamellum, and cb = cell body. (E) Comparison of average f-actin and MT movement rates before and after perfusion of CA, as determined from kymographs. b = before drug perfusion; a = after drug perfusion. Error bars represent ± standard deviation. MTs were generally not present in the lamellipodium. The scale bar in (A) represents 10 μm.

Increased Cytoskeletal Convergence Correlates with More Rapid Actin and MT Turnover

We next wanted to know whether MT and f-actin turnover were affected by pharmacological manipulations of f-actin and MT movement into the convergence zone. We performed dual-wavelength photobleaching of Cy2 MTs and X-rhodamine f-actin on a laser-scanning confocal microscope in a 10 × 10 μm region in the convergence zone of drug-treated and control cells.

In control cells, the half-time (t1/2) for recovery of MT fluorescence in the convergence zone was nearly twice as long as that of f-actin ($p < 0.01$), with both polymers showing approximately 100% fluorescence recovery (Table 1), as expected from previous studies [18, 26, 27]. In cells treated with 10 nM CA, both MT and actin fluorescence recovered significantly more quickly (actin: $p = 0.03$, MTs: $p = 0.02$) than untreated control cells (Table 1). In contrast, 10 μM ML-7 produced no effect on actin fluorescence recovery, but MT fluorescence recovery in this region was retarded (Table 1, $p = 0.017$). Comparison of the average rate of f-actin convergence (average retrograde flow + average anterograde flow rates) to the average t1/2 of fluorescence recovery from each condition revealed a negative linear relationship (Figure 5A), demonstrating that faster cytoskeletal convergence correlates with faster cytoskeletal turnover.

CA and ML-7 Do Not Affect Lamella MT Plus-End Dynamic Instability

We then wanted to determine if the changes we observed in MT turnover after drug perturbation were due to effects on lamella MT plus-end dynamic instability. Comparison of the assembly/disassembly dynamics of individual lamella MT plus ends (see Experimental Procedures) in control conditions to those of the same plus ends in the same cells after drug perfusion revealed no significant changes in the rates or durations of growth or shortening phases or the frequencies of catastrophe or rescue after treatment with either 20 nM CA or 10 μM ML-7 (Table 2).

Increased Cytoskeletal Convergence Correlates with Increased MT Breakage and Depolymerizing Minus Ends

Because our drug treatments induced no change in MT plus end dynamics, we looked to the MT minus ends. In the convergence zone and proximal lamella, we counted before and after drug perfusion both the number of mi-

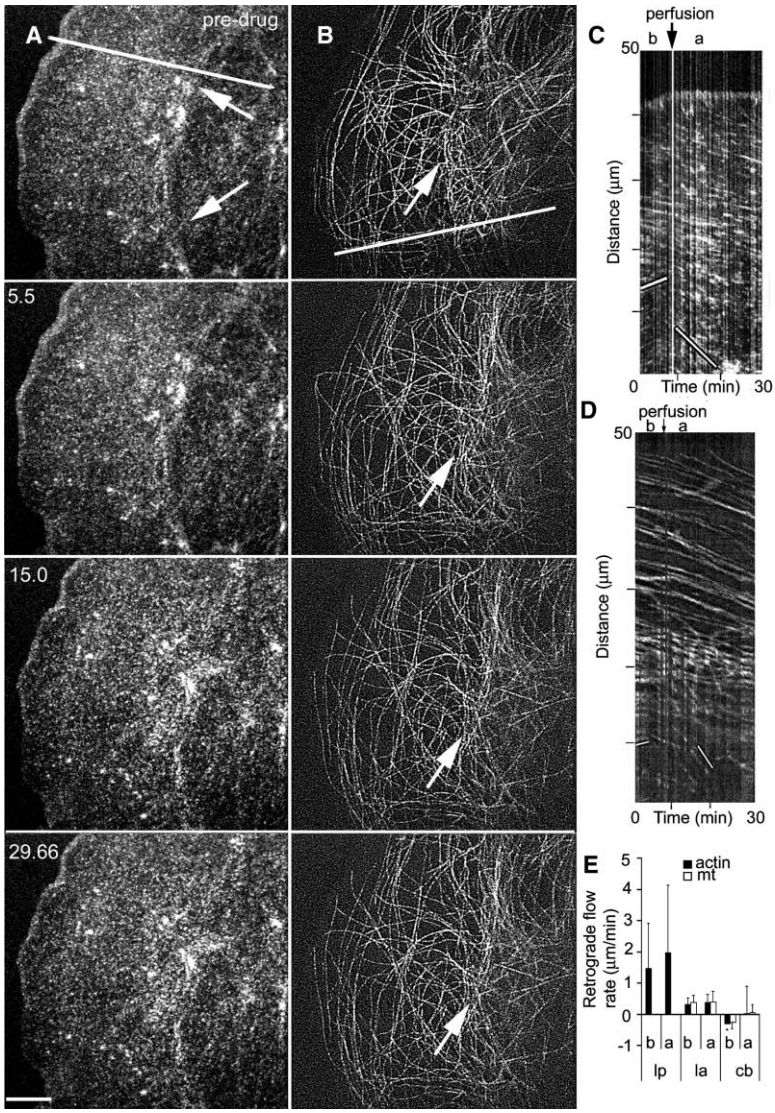

Figure 4. ML-7 Inhibits or Reverses MT and F-Actin Anterograde Flow in the Cell Body

Dual-wavelength FSM time-lapse image series of X-rhodamine f-actin ([A], left column) and Cy2 MTs ([B], right column) before and after perfusion with 10 μM ML-7. Time in minutes after perfusion is noted in the left corner of the images in (A). See Movie 4. ML-7 perfusion causes actin bundles to dissipate (arrows in [A]) and MTs to become less densely packed (arrow in [B]). White lines in (A) and (B) mark the line along which kymographs were created in (C) and (D). (C, D) Kymograph analysis of X-rhodamine f-actin speckles (C) and Cy2 MTs (D) shows that the anterograde flow into the cell body is reversed after perfusion with ML-7. Lines highlight the rates of speckle motion. lp = lamellipodium, la = lamellum, and cb = cell body. (E) Comparison of average f-actin and MT movement rates before and after perfusion of ML-7, as determined from kymographs (n = 130 measurements in six cells). Error bars represent ± standard deviation. b = before drug perfusion; a = after drug perfusion. The scale bar in (A) represents 10 μm.

nus ends produced by visible MT breakage events as well as depolymerizing MT minus ends for which we did not directly observe a breakage event (Table 3). Compared to control conditions prior to perfusion, 20 nM CA induced a significant increase both in the frequency of MT breakage ($p = 0.0003$) and the number of free minus ends ($p = 0.007$) (Table 3). Perfusion of 10 μM ML-7 induced a trend toward a decrease in both the MT breakage ($p = 0.26$) and free minus end ($p = 0.28$) frequency compared to conditions before ML-7 treatment (Table 3). A plot of average breakage or minus-end appearance frequencies from each treatment against the rate of f-actin convergence revealed a positive linear relationship (Figure 5B). This shows that faster

Table 1. Dual-Wavelength FRAP of Microtubules and F-Actin in the Convergence Zone of Migrating Newt Lung Epithelial Cells

	F-Actin		Microtubules	
	t1/2 of Recovery (min)	Fluorescence Recovery (% Pre-Bleach)	t1/2 of Recovery (min)	Fluorescence Recovery (% Pre-Bleach)
Untreated cells; n = 8	6.25 ± 2.55	114.87 ± 26.03	11.25 ± 3.94	92.12 ± 35.46
Calyculin A-treated cells, 10 nM; n = 6	3.45 ± 1.52[a]	89.75 ± 32.68	6.10 ± 2.8l5[a]	121.40 ± 57.25
ML-7-treated cells, 7.5 μM; n = 6	8.32 ± 3.35	114.83 ± 27.65	23.24 ± 12.61	76.77 ± 52.75

[a]Significantly different from untreated cells; $p < 0.01$.
Values are expressed as means ± standard deviation.

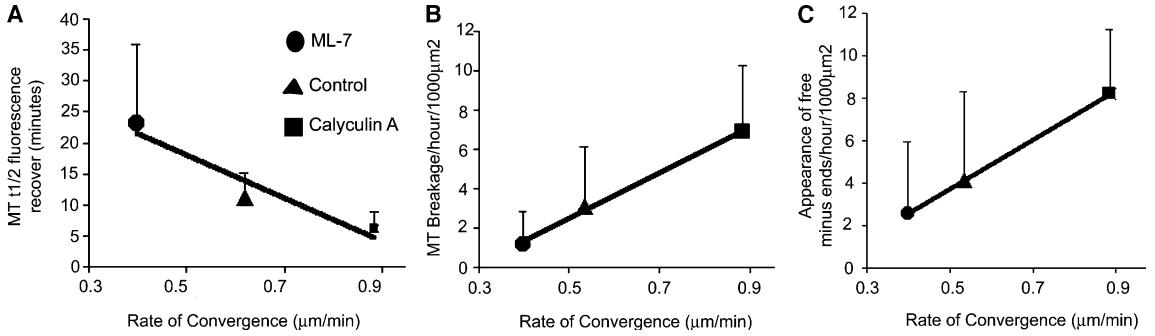

Figure 5. F-Actin Convergence Correlates with Average MT Turnover Time and MT Breakage

F-actin convergence correlates with average MT turnover time (A), average MT breakage frequency (B), and average frequency of appearance of depolymerizing minus ends (C). Data were taken from Tables 1 and 3. We calculated the average convergence rate for each treatment condition (control, CA, and ML-7) by adding the average rates of f-actin movement in the lamellum and cell body for each condition. (A) $R^2 = 0.9232$. (B) $R^2 = 0.9959$. (C) $R^2 = 1.0$.

f-actin convergence results in more MT breakage and minus end appearance.

Discussion

We have shown here that MT buckling and breakage in migrating newt lung epithelial cells is correlated with convergence of the f-actin population in the immediate vicinity of the MT. Because myosin motors power movement of f-actin in general, and particularly f-actin convergence, these results suggest that acto-myosin contractility powers MT breakage. Indeed, MT breakage occurs most frequently in the cell's convergence zone, which has a high concentration of myosin II (Figure 1). We also found that pharmacological agents that are thought to act on myosin activity manipulate the movement of f-actin and MTs into the convergence zone between the cell body and lamellum. The contraction-promoting drug, CA, induced faster movement of f-actin into the convergence zone by activating rapid retrograde flow in the lamellum, while the relaxant, ML-7, inhibited f-actin movement from the cell body into the convergence zone. This suggests that these drugs have distinct specificities, probably for different members of the myosin superfamily or different myosin II isoforms. These agents also produced corresponding changes in MT movement rates, supporting the idea that MTs may be bound or crosslinked to moving f-actin [1, 11, 14, 28]. Thus, we suggest that the crosslinking of MTs to contractile acto-myosin mediates the movements, compression, and breakage of MTs in the convergence zone and proximal lamellum.

We showed by FRAP analysis that increasing f-actin convergence sped up MT turnover without affecting MT

Table 2. Parameters of Lamella Microtubule Plus-End Dynamic Instability in Migrating Newt Lung Epithelial Cells before and after Perfusion with 20 nM Calyculin A or 10 μM ML-7

Plus-End Parameter	Pre-Calyculin A[a]	Post-Calyculin A	Pre-ML-7[b]	Post-ML-7
Growth rate (μm/min)	5.49 ± 3.06	6.28 ± 3.4	4.92 ± 4.09	5.40 ± 5.85
Growth duration (min)	0.38 ± 0.82	0.39 ± 0.39	0.37 ± 0.34	0.51 ± 0.56
Shortening rate (μm/min)	−7.65 ± 4.43	−9.345 ± 6.27	−6.28 ± 5.32	−6.96 ± 6.66
Shortening duration (min)	0.28 ± 0.18	0.30 ± 1.46	0.27 ± 0.14	0.41 ± 0.40
Catastrophe frequency (catastrophe/min)	1.88 ± 1.18	1.48 ± 0.83	1.29 ± 0.76	1.39 ± 0.79
Rescue frequency (rescue/min)	2.60 ± 1.68	2.44 ± 1.40	2.61 ± 1.61	2.32 ± 1.38

[a]n = 53 MTs in six cells for the calyculin A condition.
[b]n = 62 MTs in six cells for the ML-7 condition.
The same microtubules in the same cells were analyzed before and after perfusion. Values are expressed as means ± standard deviation.

Table 3. Numbers of Visible Microtubule Breakage Events and Free Microtubule Minus Ends in the Convergence Zone and Proximal Lamellum of Migrating Newt Lung Epithelial Cells before and after Treatment with 20 nM Calyculin A or 10 μM ML-7

	Before Calyculin A	After Calyculin A	Before ML-7	After ML-7
Breaks/1000μm²/hr	3.09 ± 3.03	6.88 ± 3.43[a]	2.04 ± 1.28	1.16 ± 1.65
Free minus ends/1000 μm²/hr	3.81 ± 3.21	8.22 ± 3.51[a]	4.41 ± 5.20	2.54 ± 2.46

[a]Significantly different from before treatment, $p < 0.01$.
Twelve cells for each condition were analyzed for 15–30 min before drug perfusion and for 30–45 min after drug perfusion. Values are expressed as means ± standard deviation.

plus-end dynamic instability at the leading edge. Because faster actin and MT convergence also correlated with increases in MT breakage and minus-end appearance frequency, the depolymerization of these minus ends in the convergence zone would need to be matched by growth in the same region to increase MT turnover rate. In light of the fact that MTs in central cell regions tend to exhibit persistent plus-end growth [29, 30], the polymerization of new plus ends created by MT breakage could be the source of some of this new polymer. However, polymer translocation into the convergence zone also probably contributes to the faster fluorescence recovery in cells treated with CA. Conversely, inhibiting actin and MT convergence could reduce MT breakage and translocation into the convergence zone, and this would slow MT turnover [11]. This suggests that changes in MT turnover rates produced by drug treatment were due to regionally regulated changes in acto-myosin-mediated MT breakage and movement in the convergence zone. Interestingly, the actin turnover rate was also increased by CA, suggesting possible regulation of actin polymerization dynamics by a myosin activity [31].

Our original hypothesis was that the depolymerizing minus ends produced by acto-myosin-mediated MT breakage in the convergence zone could serve as a source of tubulin dimers to feed net MT growth at the leading edge. We found that there are on average 41 MT plus ends facing the leading edge in a cell region comprising the lamellipodium, lamellum, convergence zone, and part of the cell body that averaged 3,254 μm^2 ($n = 10$ cells). The net growth rate that we calculated for these plus ends from our dynamic instability data was 0.33 μm/min, not surprisingly similar to the f-actin retrograde flow rate in this region ([1, 5]; this study). This leads to 13.5 μm of total plus-end net growth per lamellum per minute (0.33 μm/min $\times$ 41 MTs). On average in control conditions, we observed 10 MT breakage events for every 3254 μm^2 of lamellum every 60 min and 12 free minus ends of unknown origin that occurred on average approximately 32 μm from the leading edge. This leaves approximately 30 μm of MT in front of the labile minus end to depolymerize. Although minus ends sometimes exhibited pause, they eventually always completely depolymerized. This generates 11 μm/min of MT depolymerizing from the minus ends per lamellum (22 depolymerizing MTs $\times$ 30 μm of MT with free minus end per 60 min); this is approximately 90% of the estimated amount of net growth at the plus ends. The remaining 10 percent could come from net plus-end depolymerization in the cell body [17]. The release of MT minus ends from the centrosome of newt lung epithelial cells is negligible (approximately 3×10^{-4} MTs per min [8], and only half are oriented toward the leading edge). Therefore, the likely source of the non-breakage-associated depolymerizing minus ends is MT breakage that occurred outside the field of view or was obscured by the high density of MTs.

Calculations done in the same manner to determine if the increases in MT breakage and frequency of free minus ends induced by CA could substantially increase the amount of MT depolymerization in the convergence zone indicate that 23 μm of MTs depolymerize from minus ends per minute after treatment with CA. This is an increase of about 200% compared to the control and could account for the MT depolymerization required to double the rate of MT turnover in the convergence zone of CA-treated cells as measured by FRAP.

It is also possible that the effects on MT turnover and breakage we observed were not due solely to the action of our pharmacological treatment on f-actin and MT convergence. Alternatively, these agents could affect the phosphorylation state of MT-associated proteins (MAPs) and thereby change their affinity and thus their stabilizing effect on MTs [32]. This is unlikely because neither of the drugs had any effect on plus-end dynamic instability. Surprisingly, CA has been shown to induce depolymerization of MTs in other cell types [33], but newt lung cell MTs or MAPs appear to be resistant to the phosphatase activity of CA. Another possibility is that our pharmacological treatments could affect the activity of a MT-severing protein, such as katanin [34]. Although it is unknown if katanin activity is regulated by phosphorylation, katanin has recently been shown to act preferentially at sites of lattice defects in MTs [35]. Thus, tightly buckled MTs could be preferentially severed by katanin. However, in this case, MT breakage would still be indirectly due to mechanical stress imposed by MTs putatively bound to contracting actin filament assemblies.

Experimental Procedures

Fluorescent Protein Preparation

Cy2-labeled (Amersham Pharmacia) bovine brain tubulin and X-rhodamine-labeled chicken skeletal muscle actin were prepared as described in [36]. The final dye:protein ratio was approximately 1:1 for both proteins.

Cell Culture and Microinjection

Primary cultures of newt (*Taricha granulosa*) lung epithelial cells were established and microinjected as previously described [8]. Cells were comicroinjected with 0.5 mg/ml X-rhodamine actin and 0.2 mg/ml Cy2 tubulin as described in [1]. For FSM, cells were mounted in growth media containing 30 μl/ml Oxyrase (Oxyrase) in a custom-built perfusion chamber. For photobleaching, coverslips of cells were mounted in media supplemented with 10 μl/ml Oxyrase and either 10 nM CA or 7.5 μM ML-7 on two strips of double-stick tape placed 10 mm apart on glass slides [8]. For localization of myosin II, cells were coinjected in the nucleus with X-rhodamine actin and a plasmid encoding GFP-myosin light chain (100 μg/ml; the kind gift of Teng-Leong Chew and Rex Chisholm, Northwestern University). Within several hours, the GFP-MLC was expressed and the labeled actin was incorporated into actin structures.

Microscopy

For visualization of f-actin and MT dynamics, dual-wavelength time-lapse FSM was performed on the spinning-disk confocal microscopy system described in [37]. Using 488 nm light for Cy2 tubulin and 568 nm light for X-rhodamine f-actin, we collected one set of sequential images of the specimen in a single focal plane at 10 s intervals for 15–25 min before perfusion of either 20 nM CA or 10 μM ML-7 in media containing 30 μl/ml Oxyrase, and we then imaged the specimen for an additional 30–45 min after perfusion.

FRAP was performed on a BioRad MRC 1024 laser scanning confocal microscope system (Bio-Rad Laboratories) on an Axiovert S100 TV microscope stand with a 63$\times$ 1.4 NA Plan Apochromatic objective lens (Zeiss) and a 50 mW KrAr laser as an illumination source in the Scripps Core Microscopy facility. Simultaneous images of Cy2 MTs and X-rhodamine f-actin were collected on separate PMTs. A pre-bleach series of ten images was collected at 10

s intervals on low (<10%) laser power on 1× zoom with the confocal pinhole open maximally. The exposure area was zoomed to 10×, and an area of the convergence zone (identified by its concentration of buckled and bent microtubules) was bleached with 100% laser power. The acquisition settings were returned to pre-bleach settings, and a new image time series (20 s intervals) was begun. Total elapsed time between the end of the pre-bleach series and the beginning of the post-bleach series was 40–90 s (median = 50 s). Immunolocalization of MTs and f-actin in cells that were fixed immediately after photobleaching showed that the bleaching did not damage cytoskeletal architecture (not shown).

Image Processing and Data Analysis

All image processing and position and intensity analyses were performed with functions in MetaMorph software (Universal Imaging) and Excel (Microsoft) [1]. Kymograph analysis was performed as described [36]. For each image in the pre-bleach and recovery image series, we analyzed photobleaching recovery by recording the integrated fluorescence intensity (F_i) inside a region that was smaller than the original bleached region by 4 pixels in x and y. Calculation of the t1/2 of recovery and percent fluorescence recovery was performed as described in [38].

MT plus-end dynamic instability was measured as described in [8], except that to negate the effects of MT movement on measurements of the positions of plus ends over time, we measured the distance between the MT plus end and a speckle fiduciary mark on the MT shaft to calculate changes in MT length over time. MT plus-end change was considered to be growth or shortening if its length changed by more than 0.25 μm/time point. Changes from pause to growth (or shortening) were not considered in the calculation of rescue (or catastrophe) frequency. Growth and shortening rates and durations are expressed as averages of individual events; catastrophe and rescue frequencies were averaged for each cell. All statistical analysis was performed with a two-tailed Student's t test assuming equal variance.

Supplementary Material

Four supplementary movies are available with this article online at http://images.cellpress.com/supmatin.htm.

Acknowledgments

We thank Rex Chisholm and Teng-Leong Chew for the GFP-myosin light-chain construct, Velia Fowler for acetone powder, and Torsten Wittmann and Chris Cohan for comments on the manuscript. This work was supported by National Institutes of Health grant GM61804-01 to C.M.W.S. and a Howard Hughes Medical Institute pre-doctoral fellowship to S.L.G.

Received: July 3, 2002
Revised: August 28, 2002
Accepted: September 6, 2002
Published: November 19, 2002

References

1. Salmon, W.C., Adams, M.C., and Waterman-Storer, C.M. (2002). Dual-wavelength fluorescent speckle microscopy reveals coupling of microtubule and actin movements in migrating cells. J. Cell Biol. *158*, 32–37.
2. Wittmann, T., and Waterman-Storer, C.M. (2001). Cell motility: can Rho GTPases and microtubules point the way? J. Cell Sci. *114*, 3795–3803.
3. Small, J.V., Rottner, K., Kaverina, I., and Anderson, K.I. (1998). Assembling an actin cytoskeleton for cell attachment and movement. Biochim. Biophys. Acta. *1404*, 271–281.
4. Wang, Y.L. (1985). Exchange of actin subunits at the leading edge of living fibroblasts: possible role of treadmilling. J. Cell Biol. *101*, 597–602.
5. Waterman-Storer, C.M., Salmon, W.C., and Salmon, E.D. (2000). Feedback interactions between cell-cell adherens junctions and cytoskeletal dynamics in newt lung epithelial cells. Mol. Biol. Cell *11*, 2471–2483.
6. Cramer, L.P., Siebert, M., and Mitchison, T.J. (1997). Identification of novel graded polarity actin filament bundles in locomoting heart fibroblasts: implications for the generation of motile force. J. Cell Biol. *136*, 1287–1305.
7. Gotlieb, A.I., May, L.M., Subrahmanyan, L., and Kalnins, V.I. (1981). Distribution of microtubule organizing centers in migrating sheets of endothelial cells. J. Cell Biol. *91*, 589–594.
8. Waterman-Storer, C.M., and Salmon, E.D. (1997). Actomyosin-based retrograde flow of microtubules in the lamella of migrating epithelial cells influences microtubule dynamic instability and turnover and is associated with microtubule breakage and treadmilling. J. Cell Biol. *139*, 417–434.
9. Desai, A., and Mitchison, T.J. (1997). Microtubule polymerization dynamics. Ann. Rev. Cell Dev. Biol. *13*, 83–117.
10. Mikhailov, A., and Gundersen, G.G. (1998). Relationship between microtubule dynamics and lamellipodium formation revealed by direct imaging of microtubules in cells treated with nocodazole or taxol. Cell Motil. Cytoskeleton *41*, 325–340.
11. Yvon, A.M., Gross, D.J., and Wadsworth, P. (2001). Antagonistic forces generated by myosin II and cytoplasmic dynein regulate microtubule turnover, movement, and organization in interphase cells. Proc. Natl. Acad. Sci. USA *98*, 8656–8661.
12. Kabir, N., Schaefer, A.W., Nakhost, A., Sossin, W.S., and Forscher, P. (2001). Protein kinase C activation promotes microtubule advance in neuronal growth cones by increasing average microtubule growth lifetimes. J. Cell Biol. *152*, 1033–1044.
13. Yvon, A.M., and Wadsworth, P. (2000). Region-specific microtubule transport in motile cells. J. Cell Biol. *151*, 1003–1012.
14. Schaefer, A.W., Kabir, N., and Forscher, P. (2002). Filopodia and transverse retrograde f-actin arcs guide the assembly and transport of two populations of microtubules with unique dynamic parameters in neuronal growth cone. J. Cell Biol. *158*, 139–152.
15. Odde, D.J., Ma, L., Briggs, A.H., DeMarco, A., and Kirschner, M.W. (1999). Microtubule bending and breaking in living fibroblast cells. J. Cell Sci. *112*, 3283–3288.
16. Waterman-Storer, C.M., and Salmon, E. (1999). Positive feedback interactions between microtubule and actin dynamics during cell motility. Curr. Opin. Cell Biol. *11*, 61–67.
17. Wadsworth, P. (1999). Regional regulation of microtubule dynamics in polarized, motile cells. Cell Motil. Cytoskeleton *42*, 48–59.
18. Saxton, W.M., Stemple, D.L., Leslie, R.J., Salmon, E.D., Zavortink, M., and McIntosh, J.R. (1984). Tubulin dynamics in cultured mammalian cells. J. Cell Biol. *99*, 2175–2186.
19. Waterman-Storer, C.M., Desai, A., Bulinski, J.C., and Salmon, E.D. (1998). Fluorescent speckle microscopy, a method to visualize the dynamics of protein assemblies in living cells. Curr. Biol. *8*, 1227–1230.
20. Waterman-Storer, C.M., and Salmon, E.D. (1998). How microtubules get fluorescent speckles. Biophys. J. *75*, 2059–2069.
21. Waterman-Storer, C.M., and Danuser, G. (2002). New directions for fluorescent speckle microscopy. Curr. Biol. *12*, R633–R640.
22. Verkhovsky, A.B., Svitkina, T.M., and Borisy, G.G. (1995). Myosin II filament assemblies in the active lamella of fibroblasts: their morphogenesis and role in the formation of actin filament bundles. J. Cell Biol. *131*, 989–1002.
23. Ishihara, H., Martin, B.L., Brautigan, D.L., Karaki, H., Ozaki, H., Kato, Y., Fusetani, N., Watabe, S., Hashimoto, K., and Uemura, D. (1989). Calyculin A and okadaic acid: inhibitors of protein phosphatase activity. Biochem. Biophys. Res. Commun. *159*, 871–877.
24. Venema, R.C., Raynor, R.L., Noland, T.A., and Kuo, J.F. (1993). Role of protein kinase C in phosphorylation of cardiac myosin light chain 2. Biochem. J. *294*, 401–406.
25. Chrzanowska-Wodnicka, M., and Burridge, K. (1996). Rho-stimulated contractility drives the formation of stress fibers and focal adhesions. J. Cell Biol. *133*, 1403–1415.
26. Wang, Y.L., Lanni, F., McNeil, P.L., Ware, B.R., and Taylor, D.L. (1982). Mobility of cytoplasmic and membrane-associated actin in living cells. Proc. Natl. Acad. Sci. USA *79*, 4660–4664.
27. Kreis, T.E., Geiger, B., and Schlessinger, J. (1982). Mobility of microinjected rhodamine actin within living chicken gizzard cells. Cell *29*, 835–845.

28. Waterman-Storer, C.M., Duey, D.Y., Weber, K.L., Keech, J., Cheney, R.E., Salmon, E.D., and Bement, W.M. (2000). Microtubules remodel actomyosin networks in *Xenopus* egg extracts via two mechanisms of f-actin transport. J. Cell Biol. *150*, 361–376.
29. Vorobjev, I.A., Rodionov, V.I., Maly, I.V., and Borisy, G.G. (1999). Contribution of plus and minus end pathways to microtubule turnover. J. Cell Sci. *112*, 2277–2289.
30. Komarova, Y.A., Vorobjev, I.A., and Borisy, G.G. (2002). life cycle of Mts: persistent growth in the cell interior asymmetric transition frequencies and effects of the cell boundary. J. Cell Sci. *115*, 3527–3539.
31. Lee, W.L., Bezanilla, M., and Pollard, T.D. (2000). Fission yeast myosin-I, Myo1p, stimulates actin assembly by Arp2/3 complex and shares functions with WASp. J. Cell Biol. *151*, 789–800.
32. Cassimeris, L., and Spittle, C. (2001). Regulation of microtubule-associated proteins. Int. Rev. Cytol. *210*, 163–226.
33. Eriksson, J.E., Brautigan, D.L., Vallee, R., Olmsted, J., Fujiki, H., and Goldman, R.D. (1992). Cytoskeletal integrity in interphase cells requires protein phosphatase activity. Proc. Natl. Acad. Sci. USA *89*, 11093–11097.
34. Quarmby, L. (2000). Cellular samurai: katanin and the severing of microtubules. J. Cell Sci. *113*, 2821–2827.
35. Davis, L.J., Odde, D.J., Block, S.M., and Gross, S.P. (2002). The importance of lattice defects in katanin-mediated microtubule severing in vitro. Biophys. J. *82*, 2916–2927.
36. Waterman-Storer, C. (2002). Fluorescent speckle microscopy (FSM) of microtubules and actin in living cells. In Current Protocols in Cell Biol. (New York: John Wiley & Sons), pp. 4.10.1–4.10.26.
37. Adams, M.C., Salmon, W.C., Gupton, S.L., Cohan, C.S., Wittmann, T., Prigozhina, N., and Waterman-Storer, C.M. A high-speed multi-spectral spinning disc confocal microscope system for fluorescent speckle microscopy of living cells. Methods, in press.
38. Bulinski, J.C., Odde, D.J., Howell, B.J., Salmon, E.D., and Waterman-Storer, C.M. (2001). Rapid dynamics of the microtubule binding of ensconsin in vivo. J. Cell Sci. *114*, 3885–3897.